A Review of Thermal Runaway Prevention and Mitigation Strategies for Lithium-ion Batteries

Sunil BanduDhas
PG Scholar, Department of Mechanical Engineering,
Dhole Patil College of Engineering, Wagholi, INDIA
sunil.dhas83@gmail.com
Prof.Anantharama Baipadithaya
Professor, Department of Mechanical Engineering,
Dhole Patil College of Engineering, Wagholi, INDIA
baip1066@gmail.com

Publication History
Manuscript Reference No: IJIRAE/RS/Vol.11/Issue01/JAAE10084
Research Article | Open Access | Double-Blind Peer-Reviewed | Article ID: IJIRAE/RS/Vol.11/Issue01/JAAE10084
Received: 04, January 2024 | Revised:14, January 2024 | Accepted: 24, January 2024 || Published Online: 31, January 2024
https://www.ijirae.com/volumes/Vol11/iss-01/08.JAAE10084.pdf
Article Citation: Sunil,Anantharama (2024).A Reviewof Thermal Runaway Prevention and Mitigation Strategies for Lithium-Ion Batteries. IJIRAE::International Journal of Innovative Research in Advanced Engineering, Volume 11, Issue 01 of 2024 pages 53-63 **Doi:>** https://doi.org/10.26562/ijirae.2024.v1101.08
BibTeX Sunil2024@Review
Academic Editor-Chief: Dr.A.Arul Lawrence Selvakumar, AM Publications, India

Abstract: Lithium-ion batteries are widely considered the leading candidate energy source for powering electric vehicles due to their high energy and power densities. The thermal runaway of lithium-ion batteries is the phenomenon of chain exothermic reactions within the battery. These reactions cause a sharp rise in the internal battery temperature causing the inner structures of the battery to destabilize and degrade, which eventually leads to the failure of the battery. This study thermal runaway initiation mechanisms, thermal runaway propagation, Thermal runaway is a major safety concern; therefore, the development of mathematical and numerical experimental models to predict thermal runaway is reviewed, which provides useful data to design and develop battery packs with thermal runaway safety features.It explores the importance of effective battery thermal management systems to prevent thermal runaway and reviews strategies for mitigating damages in case of an occurrence.

I. INTRODUCTION

A lithium-ion battery may experience mechanical abuse if the external stress causes the battery to deform or become punctured by some sharp items. Additionally, due to overcharge, over discharge, and external short circuit, lithium-ion batteries may not adhere to their fundamental electrical properties. This could result in electrical abuse of lithium-ion batteries. Also, lithium-ion batteries may overheat due to internal electrochemical side reactions or external heat sources heating up, leading to thermal abuse of lithium-ion batteries. All these elements have the potential to cause a succession of exothermic reactions in lithium-ion batteries within minutes, which would cause a sharp rise in the internal temperature of battery. This would then likely result in a thermal runaway event, which would typically result in smoke, fire, or possibly an explosion [2],[4]. Thermal runaway events represent a serious hazard to human life and property in the form of smoke, fires, and explosions [5],[6]. to gauge the safety of lithium-ion batteries to enhance their performance and safety as well as allay concerns about thermal runaway [7],[8]. To ensure the quality and safety of lithium-ion batteries used, these specifications mandate that lithium-ion batteries must pass safety verification tests, such as overcharge, over discharge, overheat mechanical shock, and other tests. They also stipulate that the test cannot expose the battery to any secondary hazards (leakage, fire, explosion, etc.). Abuse from a variety of sources is frequently inevitable. The development and acceptance of electric vehicles, electric ships, and lithium-ion batteries has all been significantly hampered by the growing serious safety issue with lithium-ion batteries. Consequently, the battery's own perspective, one method is to improve the production process within the lithium-ion battery itself by adding electrolyte additives, improving electrode materials, and improving the separator preparation process; an alternative method is to take changes in voltage, internal resistance, temperature, and other parameters accompanying the process of thermal runaway of lithium-ion batteries into consideration from the perspective of monitoring and warning to achieve the purpose of reducing casualties. As analysis and forecast of the likely direction of future development for battery monitoring, warning, and protection technologies.

II. THERMAL RUNAWAY CHARACTERIZATION

The characterization of thermal runaway consists of thermal runaway mechanisms, propagation, and gas characterization. The underlying mechanisms that establish thermal runaway comprise mechanical, electrical, and thermal abuse mechanisms.

Nomenclature

c_p	specific heat capacity (J kg^{-1} K^{-1})
T	temperature (K)
t	time (s)
k_T	effective thermal conductivity (W/m K^{-1})
Q	heat generation (W)
I	current (A)
E_j	equilibrium potential (V)
V	battery working voltage (V)
E	energy (J)
P	pressure (Pa)
h_j	Enthalpy of species in the specified phase (J)
S_h	Volumetric heat sources (W)
k	turbulence kinetic energy (J kg^{-1})
x	x-direction
G_k	production of turbulent kinetic energy
G_ω	generation of specific dissipation rate
Y_k	dissipation due to turbulence for turbulent kinetic energy
Y_ω	dissipation due to turbulence for specific dissipation rate
ρ	density (kg m^{-3})
$\vec{v}$	velocity (m/s)
$\bar{\bar{\tau}}$	stress tensor
Γ_k	effective diffusivity of turbulence kinetic energy
Γ_ω	effective diffusivity of specific dissipation rate
ω	specific dissipation rate (s^{-1})

Abbreviations

GHG	Greenhouse gas
EV	Electric vehicle
PHEV	Plug-in hybrid electric vehicle
BEV	Battery electric vehicle
Li-ion	Lithium-ion
LMO	$LiMn_2O_4$
LCO	$LiCoO_2$
LFP	$LiFePO_4$
LTO	Lithium titanate
NMC	Lithium nickel manganese cobalt
NCA	Lithium nickel cobalt aluminum
ISC	Internal short circuit
ESC	External short circuit
SOC	State of charge
ARC	Accelerating rate calorimetry
EV-ARC	Extended volume-accelerating rate calorimetry
TNT	2,4,6-trinitrotoluene
BTMS	Battery thermal management system
DSC	Differential scanning calorimetry
SEI	Solid-electrolyte-interface
PCM	Phase change material
EG	Expanded graphite
GcN	Graphene coated nickel
HP	Heat pipes

Once thermal runaway occurs at the battery level, it begins to propagate to the neighboring batteries and subsequently through the entire battery pack. The thermal runaway characterization also includes the details of vented gases during thermal runaway. These gases are a potential health and safety hazard, and it is vital to study the different gases present and their corresponding amounts.

A. Thermal runaway mechanism

1] Mechanical abuse

The two common characteristics of mechanical abuse are destructive deformation and destructive displacement due to an applied force. When a vehicle collides or crashes, the battery pack is likely to either be crashed or penetrated by an external object. This causes the separator between the cathode and anode of the battery to tear away, resulting in an internal short circuit (ISC). The mechanical abuse phenomenon from a structural point of view was investigated by Zhu et al.[16]. An experimental study on quasistatic loads, low-velocity punch penetration, and wedge-cutting tests were carried out. The battery module consisted of 18 sub-assemblies and two cover plates at the top and the bottom of the battery pack. The subassemblies included pouch batteries, cooling plates and cushions. It was concluded that the punch penetration test resulted in higher forces and increased absorption of energy due to the higher degree of material densification. Similarly, Hu et al.[17]conducted an experimental study on 18,650Li-ion batteries to study the effects of dynamic collision and quasi-static compression. The results showed that cylindrical batteries in a pack behave differently than individual batteries under crushing scenarios. The results indicated that the dominating property in the dynamic collision was the crushing velocity rather than the crushing energy. Once the crushing velocity exceeds 20 m/s, the battery pack failure switches from initial failure at the last row to initial failure at the first row. In addition to the crushing mechanisms, the penetration mechanisms also cause ISC, which leads to the thermal runaway of the Li-ion batteries. Yamauchi et al. [18] investigated the penetration mechanism and concluded that the electrical energy of the battery is constantly released during the ISC caused by penetration. The battery's temperature also continuously increases by heat generation due to the ISC until the battery discharges. At the end of this process, if the temperature fails to reach the critical level, then there is no thermal runaway. In another study, Maleki and Howard [19] examined the discharging of the battery under the ISC caused by the penetration mechanism. The results concluded that within the first minute of ISC, 70 % of the energy was released; due to which a sharp temperature increase was noticed. Additionally, the location of the battery penetration also affects the thermal runaway characteristics. For example, in instances where the penetration occurred at low heat dissipation locations, the risk of thermal runaway increased significantly. To understand the flow of current during the penetration mechanism, Zavala's et al. [20] developed a 2D numerical model for a prismatic battery and studied the mechanism. The results of the study concluded that the maximum temperature increase during the thermal runaway was restricted by the mass transport of Li-ions in the electrolyte. Moreover, there are two mechanisms through which a short circuit occurs during penetration. In the first mechanism, the current passes through the penetrating object (ISC) and in the second mechanism, the current passes through the electrodes (external short circuit). When the penetration occurs, 75 % of the current passes through the electrodes, and 25 % passes through the penetrating object. Moreover, Zhao et al. [21] studied the effects of the capacity of the battery on the ISC during the nail penetration process. The results concluded that with the increase in the battery capacity, the current flow increased at the nail penetration location. This led to extensive heat generation and, subsequently, thermal runaway. Zhu et al. [22] conducted mechanical abuse studies on the Li-ion jelly rolls and prismatic batteries under quasi-static loads. Hemispherical nose, round edge wedge, and flat end indenters were used to apply the loads on both types of batteries.

For jelly roll batteries, the hemispherical nose and flat end indenters showed a penetration type commonly seen in porous media with a hole at the contact point followed by a tunnel. With the round edge wedge indenter, a "/" and "V" crack appeared on each layer of the jelly rolls. Similar results were seen by using the hemispherical nose and flat end indenters on the prismatic batteries. However, with the wedge indenter, the enclosure of the prismatic battery was not penetrated when the same force was applied. The results from the experiments also showed that once the ISC occurs on the first layer of the jelly roll, the entire battery fails.

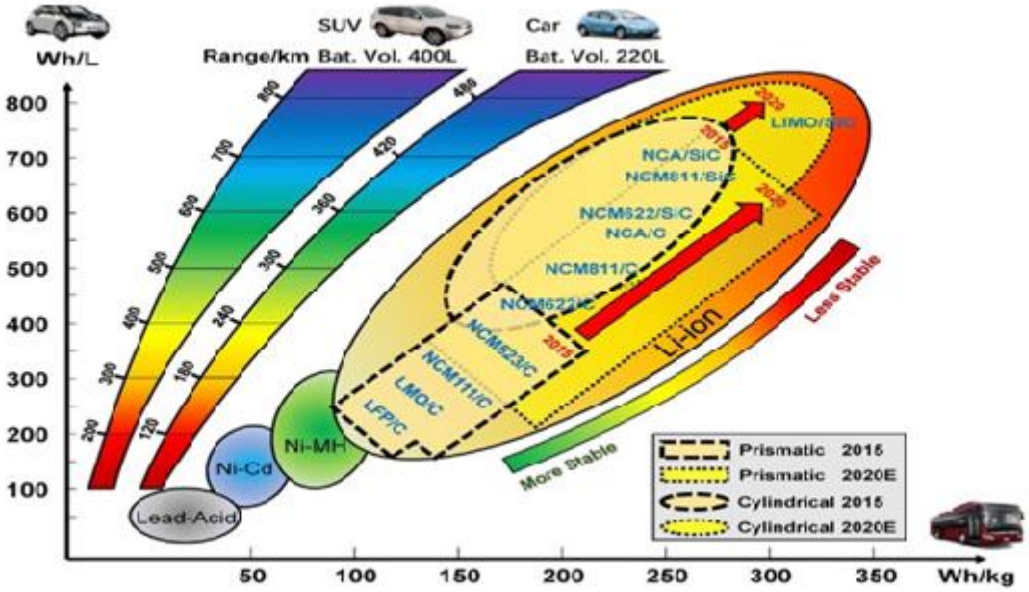

Fig. 2. Roadmap of EV batteries

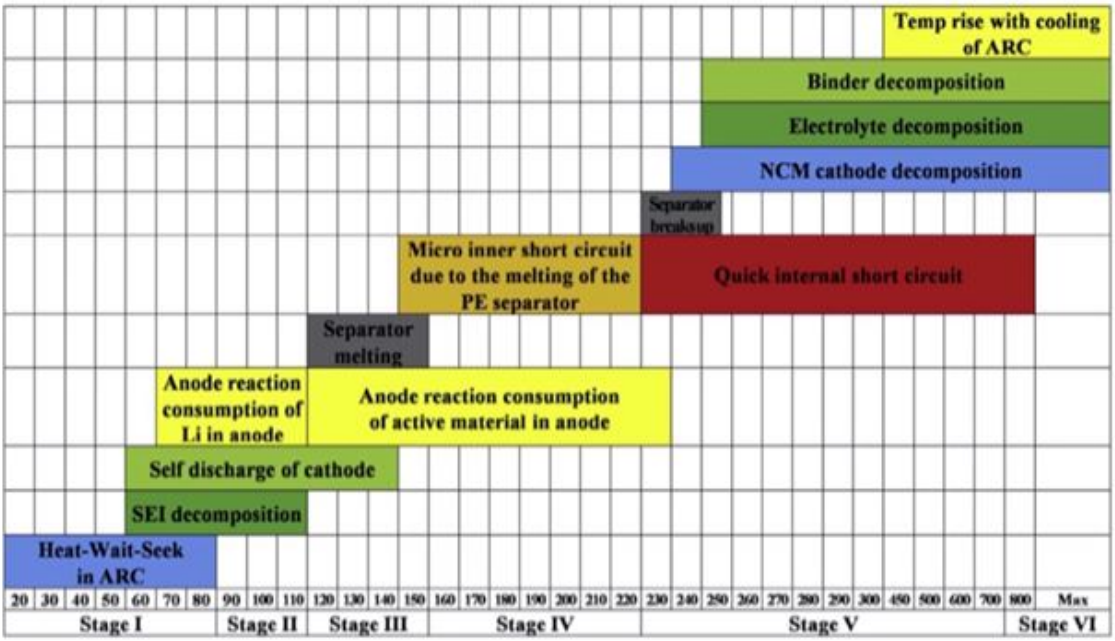

Fig. 3. Various stages of thermal runaway during an ARC testing

2] Electrical abuse

The external short circuit (ESC) of the batteries is considered one of the causes of electrical abuse. It occurs either due to exposure to water, conductor contamination, electric shock, or the deformation of the battery during mechanical abuse. The ESC was investigated by Leising et al. [23], where the current was increased to its peak value and then rapidly decreased to a plateau before reducing to zero to complete the discharge process of the battery. The temperature increased sharply with the increase in current. Once the plateau current was reached, there was no further increase in temperature; hence, the thermal runaway did not occur. To trigger thermal runaway due to an ESC, either the mass transfer coefficient for Li-ion at the anode or the surface area of the anode had to be increased. Both cases cause a higher current flow and subsequently rapid heat generation [24]. On the contrary, overcharging the Li-ion battery can lead to worse thermal runaway consequences due to the excessive energy in the battery.

Once the battery is overcharged, the heat generation increases, and large amounts of joule heating and side reaction heating at the anode and the cathode occurs, resulting in a sharp increase in the battery temperature [25],[26].Ohsaki et al. [27]studied LCO prismatic batteries with a graphite anode. Several gases, including CO2, CO, C2H6, C2H4, and H2 were released during the overcharge of the batteries. The volume of gases increased with the increase in the temperature of the battery. The results also showed that once the temperature of the battery increased beyond 60 ◦C the exothermic oxidation reaction at the electrolyte increased quickly, causing the overall battery temperature to increase sharply. The authors concluded that the thermal runaway occurred due to the violent reaction between the overcharged anode (lithium deposition) and the electrolyte solvent at a high temperature which occurs due to the exothermic reaction between the cathode and electrolyte. Yuan et al. [28] studied the behavior of the prismatic battery under overcharge conditions. The internal and external temperatures of the battery were monitored. The results showed that when the battery is overcharged to the maximum voltage of 5.10 V, the internal temperature of the battery goes up to 50 ◦C, and electrolyte oxidation occurs. With further overcharge (greater than180 % State of Charge), the interface between the cathode and electrolyte becomes highly reactive, and the internal temperature of the battery increases above 200 ◦C. The thermal runaway occurs due to the lithium plating on the anode during the overcharge of the battery. Ye et al. [26] conducted an experimental study on prismatic batteries. The results indicated that the side reactions result in an 80 % heat generation during overcharge. Furthermore, if the charging current is more than 1C, then effective cooling methods should be employed within 2 min once the inflection point voltage is surpassed to prevent thermal runaway. The maximum internal temperature during thermal runaway exceeds 660 ◦C. Mao et al. [29] conducted an experimental study to analyze the changes in the internal composition of the batteries. The results showed that thermal runaway is more likely to be triggered under adiabatic conditions rather than under ambient environmental conditions. It was also concluded that the cathode is prone to get highly reactive when the battery is overcharged to 150 % state of charge (SOC), and the heat generated and released was 1026.4 J/g. To supplement the studies of overcharge effects on the Li-ion batteries, Hamisi et al. [30] developed a 2D electro thermal model for 18,650 cylindrical batteries. Through numerical studies, it was found that the heat distribution within the battery tends to stay uniform. The total heat generation rate increases with increasing the overcharge current due to an increase in the joule heating of the battery. Finally, with a 5C charging current, the battery surface temperature increases sharply compared to lower C-rate charging currents. Yeh et al. [31] further studied the overcharge mechanism and its effects on the separator of the Li-ion batteries. The separators are usually manufactured using thermoplastic materials. The composite material consists of polypropylene/polyethylene/polypropylene layers. During overcharge, once the temperature rises, the irregular crystalline structure of the polyethylene layer melts, resulting in interface disturbance and partially blocking the Li-ion channel. This causes the Li-ion to follow through alternate channels, which results in a sharp increase in the voltage.

3]. Thermal abuse

The causes of thermal abuse within Li-ion batteries and battery packs include overheating due to mechanical and/or electrical abuse and overheating due to improper connections and contacts of batteries. Thermal abuse causes an increase in the battery's internal and external temperatures, which can melt the separator between the anode and the cathode, resulting in ISC. This increases the temperature quickly, risking a potential thermal runaway. The different stages of a thermal runaway due to thermal abuse during accelerating rate calorimetry (ARC) testing are shown in Fig. 3. Feng et al. [32] conducted extended volume-accelerating rate calorimetry (EV-ARC) tests on large format prismatic batteries. The results indicated that the thermal runaway occurs approximately at 520 ◦C. The instantaneous temperature rise occurs about 15–40 s from the sharp drop in voltage. Additionally, before thermal runaway, the internal resistance of the battery increases from 20 mΩ to 60 mΩ. Once thermal runaway occurs, the internal resistance rises to 370 m (about 1213.91 ft) Ω. which indicates the melting of the separator and the swelling of the battery [32].

Wu et al. [33] conducted an ARC test to compare the thermal runaway of prismatic batteries under internal and external heating modes. The results indicated that the duration of the thermal runaway reduces as the operating current increases in the internal heating mode. On the contrary, the duration decreases as the SOC increases during external heating mode. However, in both heating modes, the voltage drops sharply a few minutes before the rapid temperature rises. The onset and critical temperature are higher in the external heating mode compared to the internal heating mode. Zhao et al. [34] conducted EV-ARC test of cylindrical batteries by using different SOC and cycling times to study the thermal runaway hazards. The battery was subjected to a ramp heating method to depict thermal abuse conditions. The results showed that the internal pressure and the maximum surface temperature of the battery increased with the SOC increase when thermal runaway occurred. The authors calculated the energy release of the completely charged fresh battery to be 61.72 kJ. This energy release is equivalent to a 5.57 g, 2,4,6-trinitrotoluene (TNT) explosive. Additionally, aged batteries, when compared to fresh batteries, are more prone to trigger thermal runaway.

III. EXPERIMENTAL SECTION

The thermal runaway tests were performed on a commercial 28.8 Ah pouch cell with an energy density of 205 Wh/kg. This cell has Li (Ni0.5 Co 0.2 Mn0.3) O 2 as its cathode, graphite as its anode, and polyethylene (PE) with ceramic coating on one side as its separator, with the specifications listed in Table 1. This cell is used to investigate on the thermal runaway characteristics in an adiabatic environment after charged at different rates.

Table I. Materials, Mass(m), Specific Capacity(c_s), and Heat Capacity (c_p) of the Battery.

components	materials	m (g)	c_s [mAh g^{-1}]	c_p [J $kg^{-1}K^{-1}$]
cathode	NCM523	206.5	161	1270[52]
anode	graphite	118.6	310	1437.4[53]
separator	PE/ceramic	18.1		1978[52]
electrolyte	$LiPF_6$/EC + DMC + EMC	75.5		133.9[53]
current collector	copper	46.0		385[53]
	aluminum	22.5		903[53]

A. Performance Tests for Charging.

The charging performance tests (CPTs) were implemented with three stages: the standard capacity test I (SCT I), the charging rate test II (CRT II), and the discharge capacity test III (DCT III). During the three stage tests, the fading characteristics were measured for cells charged at elevated rates. Besides, after experiencing the CRT II, the cells were prepared for the ARC tests and partial cell fabrications. The detailed profiles of CPTs are listed in Table 2. SCT I was first performed on cells to measure the capacity with a constant-current constant-voltage (CCCV) charging and constant-current (CC) discharging. After that, CRT II was followed to examine the charging performance of the cells at different charging cases. The different charging cases include the low-rate charge case with C/3 charging, the mid-rate charge case with 1.5C charging, and the high-rate charge case with 3C charging. In addition, fully charged cells were obtained with a CCCV charging at the end of CRT II. Finally, DCT III was carried out with CC discharging to measure the capacity retention of the cells. All the tests in CPTs were conducted in a temperature chamber at 25 °C.

B. ARC Tests.

The thermal runaway tests were conducted in an extended-volume accelerated rate calorimetry (EV+ARC) system that was produced by Thermal Hazard Technology to evaluate battery safety behaviors. The ARC tests were first conducted on full cells to compare the thermal runaway behaviors of cells at different charging cases. Next, the cells at high-rate charging cases were examined. Their corresponding partial cells were tested by EV+ARC to explore the thermal runaway mechanisms. In the experiments, the cell was hung by iron wires inside the ARC for the thermal runaway tests, as shown in Figure 1. A pair of aluminum strips were applied to fix the thermocouple at the center of the cell surface. To ensure the repeatability of thermal runaway, the ARC tests are performed within 1 h after the cells are charged. The voltage and temperature of the cells are recorded with a time interval of 1 s. A heat–wait–seek method is operated on the ARC.

C. Partial Cells Preparation and Tests.

In this study, partial cells, derived from incomplete batteries dissected from full cells, play a crucial role in understanding the intricate thermal runaway mechanisms of lithium-ion batteries.

Table II. Profits for the CPT_s

test section	step no.	step name	duration	condition
standard capacity test I (SCT I)	1	rest	60 min	
	2	CCCV charge		C/3 until 4.2 V, then 4.2 V until I < C/20
	3	rest	60 min	
	4	CC discharge		1C until 2.8 V
	5	rest	60 min	
	6	cycle	2	steps 2–5
charging rate test II (CRT II)	7	CC charge		C/3 until 4.2 V for low-rate charge case; or 1.5C until 4.2 V for mid-rate charge case; or 3C until 4.2 V for high-rate charge case
	8	rest	60 min	
	9	CC discharge		1C until 2.8 V
	10	rest	60 min	
	11	CC charge		C/3 until 4.2 V for low-rate charge case; or 1.5C until 4.2 V for mid-rate charge case; or 3C until 4.2 V for high-rate charge case
	12	rest	10 min	
	13	CCCV charge		C/3 until 4.2 V; then 4.2 V until I < C/20
discharge capacity test III (DCT III)	14	rest	60 min	
	15	CC discharge		1C until 2.8 V

These partial cells are categorized into anode-electrolyte (AnEle), cathode-electrolyte (CaEle), and anode-cathode (AnCa) partial cells, each designed to isolate specific subsystems for analysis. The thermal runaway behaviour is explored within three thermodynamic systems: anode-electrolyte, cathode-electrolyte, and separator-electrolyte. To simplify the interpretation of thermal runaway mechanisms, partial cells with removed subsystems are employed. AnEle partial cells focus on the anode-electrolyte system, while CaEle partial cells concentrate on the cathode-electrolyte system. AnCa partial cells, with the electrolyte removed, investigate the interaction between the cathode and anode.

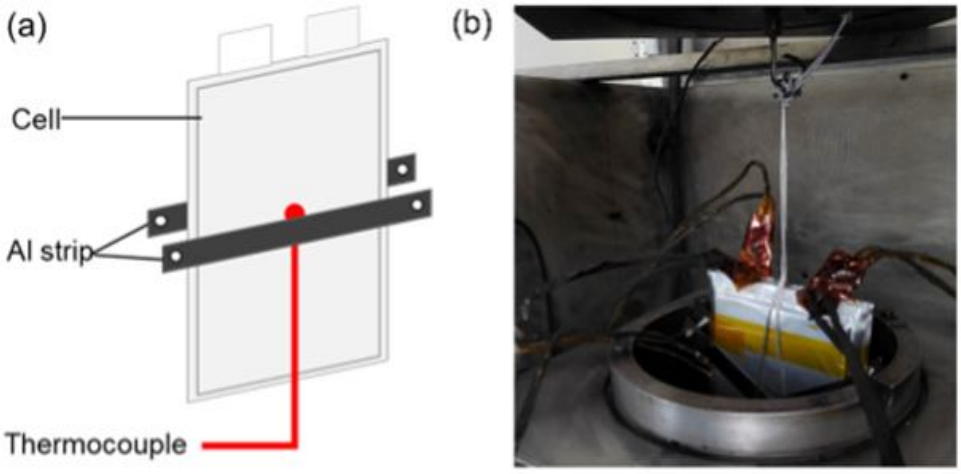

Fig 1. Experimental setting for the ARC tests. (a) Installation of the thermocouple at the center of the cell surface; (b) installation of pouch cells in the EV +ARC.

The preparation process involves meticulous disassembly of full cells, ensuring repeatability and minimizing side reactions during rest. The detailed procedures include dismantling, removal of specific components, and repackaging within controlled environments. These partial cells serve as essential tools for analysing individual reactions and understanding the complex interplay of subsystems in lithium-ion batteries thermal runaway.

D. DSC Tests.

The DSC tests were conducted with a Netzsch DSC214 Polyma system with the temperature rising from 50 to 450°C at a rate of 10 °C/min. As the temperature rises, the heat release rate was measured to assess the thermal stability of the test samples. Test samples were mixtures of battery's active materials, which were obtained from disassembling fully charged cells after different rates. To obtain the materials, the dismantled electrodes were first cleaned by DMC and repeatedly dried in an argon atmosphere to minimize he residual electrolyte on the electrodes. After that, the electrodes were scratched by a scalpel to obtain active materials on the current collectors. The active materials were thoroughly ground by an agate mortar to ensure the uniformity of the sample powder. Finally, the sample powder was packed and sealed in the crucible with a consistent ratio in the cells. The ratio of anode to cathode in cells is 3.5:2 mg/mg, with 2 L of electrolyte, as listed in Table 1. Before the crucible was loaded into the DSC, a pinhole was pierced on the crucible lip to provide a stable pressure inside the crucible with increasing temperature. The preparation process was performed in an argon glovebox to avoid the influence of air during the test. DSC tests are performed sequentially on pure anode and mixed anode with electrolyte. The thermal stability of anode materials from cells charged at a high rate is first compared with that from cells charged at a low rate. Furthermore, the anode materials near the current collectors are tested to determine the reactants in the anode charged at the high rate.

3.5. Scanning Electron Microscopy and Nuclear Magnetic Resonance.

A Zeiss Merlin field-emission scanning electron microscopy (FE-SEM) instrument with a secondary resolution of 0.8 nm at 15 kV accelerating voltage is implemented to observe the morphology of electrode. The SEM images of anodes charged at different rates are compared to evaluate the severity of lithium plating. A 600 M nuclear magnetic resonance (NMR) instrument produced by JEOL is used to measure the content of lithium metal in anode powders. The sample powder, sealed into the rotor of NMR, isrotated with a spin frequency of 12 kHz at a spin angle of 54.74°. TheNMR spectrum is measured from −100 to 300 ppm in reference to the LiCl powder with a pulse delay of 20s.

IV. TR DETECTION METHODS

In addition to balancing voltage and SOC, a BMS has to detect the onset of TR. Most simply, this can be done by measuring the temperature of the battery cells. One of the main challenges is the difficulty of measuring the temperature of individual cells and acquiring their internal (core) temperature. This would allow earlier measures to be taken before damage or TR occurs, as the increase in temperature occurs internally before it increases externally. A noninvasive method has been proposed, which uses energy conservation equations to determine the core temperature of a cylindrical cell from its outside surface temperature distribution.[52] The results (Figure 3a) showed close agreement with a battery with an actual set of thermocouples inside. Another publication developed models to produce estimations of temperature distribution throughout the battery in real time utilizing a Kalman filter and a tuned thermal model with finite temperature sensors.[53] However, so far, most models of TR are based on the surface temperature of the cell which can be directly measured. Studies of the evolution of the battery surface temperature (Figure 3b) show that there are different stages.[54],[55] The SEI decomposition starts at *T*1, and the melting process of the separator begins at *T*2 (usually 130–160 °C). Above this temperature, the separator loses its mechanical integrity and starts to induce internal micro-short circuits. The point *T*3 is the TR trigger (or critical) temperature, which initiates an exponential increase in temperature caused by the exothermic reactions and short circuits.

This temperature is usually under 200 °C,[54, 55] but this will depend on battery chemistry,[51] as well as SOC,[56] thermal transport within the cell, thermal transport from the cell surface to the outside, and the cell geometry.[57]

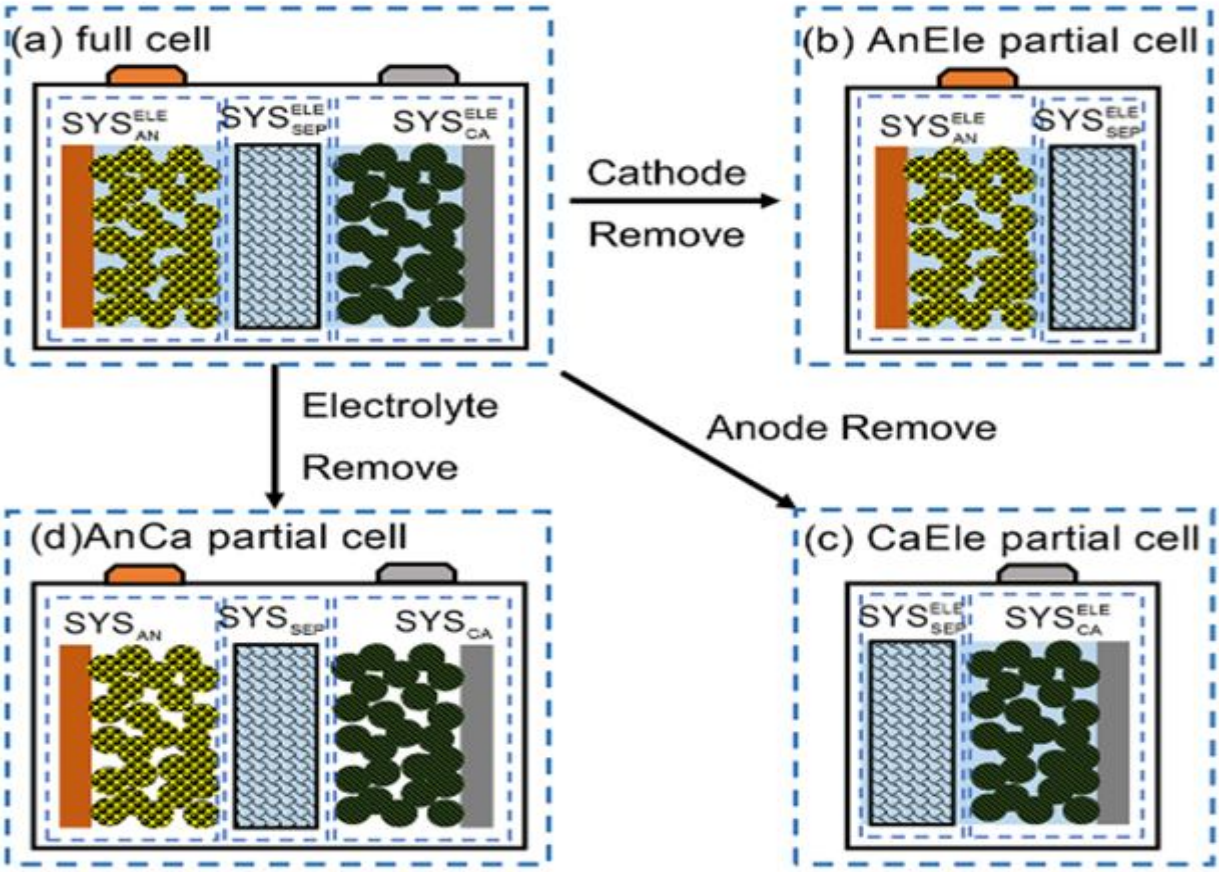

Fig 2.Thermodynamics system of the full cell and the patial cell:
(a) full cells ,conttining the anode-electrolyte system, cahode-eclectrolyte system, and separator-electrolyte sysem;
(b) AnEle partial cells; (c) CaEle partial cells; (d) AnCa partial cells.

Temperatures under *T*1 are within the safe operating area, and temperatures under *T*3 can potentially be considered "reversible" areas, although the severity of the damage inside the cell increases with increasing temperature. It has been observed that *T*1 increases and *T*3 decreases as the cell ages.[58] A combination of experimental work with modeling[53], [55], [59] concluded that *T*2 is critical for evaluating battery safety, because a cell with higher *T*2 will be more likely to pass abuse tests, such as oven heating, nail penetration, or other mechanical abuse.[60], [61] Measurements other than temperature could be used by the BMS to detect the state of health of a battery cell. For example, in situ impedance characterization in real time observed that the Warburg element of cell impedance was particularly sensitive to increased operation temperature.[58] Impedance measurements of charge-transfer resistance are emerging as a low-cost method for the BMS to monitor the state of health of cells during use.[62] Some of the newer BMSs use incremental capacity analysis to assess the battery state of health. If the state of health is defined by the maximum capacity of the cell as a percentage of the original maximum capacity, then capacity readings should give an idea of state of health with each cycle. However, batteries are rarely fully discharged, with vehicles usually operated at 40–80% depth of discharge.[63] The BMS can use algorithms to calculate the state of health from standard sensor inputs (voltage, current, and temperature) in real time. These algorithms are based on the derivative of the partial charging curve with respect to the cell voltage.[63],[64] Compared with other computational methods of estimating capacity in real time, such as Kalman filter-based algorithms and machine learning, relatively small amounts of experimental data and computational power are required.[65] Noninvasive analysis methods can also be used to detect specific battery failure events from the battery voltage reading over time. For example, weakened contacts in the electrical circuitry surrounding the battery can be detected by statistical comparison with an equivalent circuit model,[66] and lithium plating at the anode can be inferred by identifying a characteristic stripping plateau at the discharging plateau of the battery.[67] Another approach to TR detection by the BMS is to detect gas release. An increase in temperature and gassing both increase pressure inside the cell, and gas sensors can be used in tandem with volume expansion measurements (via pressure sensors) of cells to detect gas evolution in the earliest stage of TR (SEI decomposition).[68] The exact quantity and composition of gas evolved during decomposition of the SEI depend on cell chemistry, but because of unavoidable impurities, lithium carbonates are present at the cathode SEI and residual water at the anode SEI; this means that all lithium-ion batteries will generate CO2 and H2 in measurable concentrations.[24], [69]

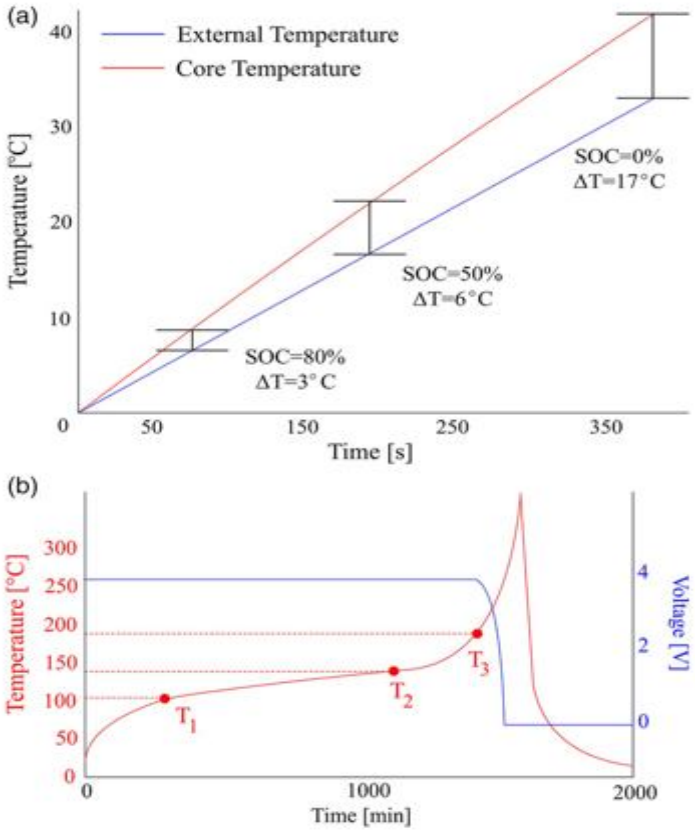

Fig. 3a) Theoretical relationship between the external and core temperature of a cell.[52]
b) External temperature and voltage of a battery cell.[54]

Evaporated electrolyte can also be detected by sensors for volatile organic compounds.[70] Results of implementing a gas sensor into a lithium-ion battery system [71] show that the sensors can detect electrolyte leaks and an increase in volatile organic compound concentration and can detect battery failures earlier than the temperature sensors. However, it is still unclear if this is always effective as success varies according to sensor position and sensitivity, mechanical restrictions in the battery system, and decomposition onset temperature. Ideally, the sensors would detect the gases at ppm levels, but in practice, this is challenging.[72]

V. TEMPERATURE-SENSITIVE ADDITIVES (POSITIVE TEMPERATURE COEFFICIENT [PTC] MATERIALS)

Certain ferroelectric semiconductors have a positive temperature coefficient (PTC) relationship between resistivity and temperature and become dramatically less conductive above their Curie temperature,[112] the point at which there is an abrupt change in the crystal structure of the material. This means that if these materials are used as the conductive additive in lithium-ion battery electrodes, the cell conductivity could undergo a several orders of magnitude decrease above a certain temperature. The great challenge is to find a material with a Curie temperature close to room temperature; most materials have a temperature well above 200 °C. The class of materials used in ceramic PTC resistors has the general formula Ba1−*x*LnTiO3, where Ln is a metal from the lanthanide series. For example, recently Ba0.7Sr0.3TiO3 and Ba0.9Sr0.1TiO3 ceramics displayed Curie temperatures of 38 and 54 °C, respectively, which are only just below the onset temperature of TR.[113] Ceramic PTC materials are only semiconducting (the conductivity of BaTiO3 is close to 10−7 S cm−1 at room temperature)[114] so require the addition of a conductive additive (Table 4). Apart from conductive additives, the polymer binders inside the cell can also be designed as temperature sensitive, ideally beginning at temperatures below 100 °C. For example, LiCoO2 sandwiched with poly(methyl methacrylate) mixed with Super P carbon black was found to have PTC properties, increasing resistance at 80–120 °C such that the cell capacity of 140 mAh.g−1 decreases to 8.4 mAh g−1 at 110 °C, blocking transfer of most of the current through the cell.[115] Carbon/polyethylene composites are another PTC material;[116] the challenge is to improve the contact between the conductive particles embedded in the polymer matrix.

Table 4. Properties of recent PTC materials for lithium-ion batteries. RT = room temperature

Material	PTC Temp range [°C]	RT conductivity	Order of magnitude decrease in conductivity/increase in resistivity
Poly(3-octypyrrole)/C	120	30.3 Scm^{-1}	4
Poly(3-doddecylthiophene	90–100	–	4
Polyethylene microspheres	110	0.3 $mScm^{-1}$	Not measured

Poly(3-ethylenedioxythiophene) (PEDOT/C)	100–120	600 Scm^{-1}	>4
PVDF/Ni nanoparticles	75–170	300 Scm^{-1}	8
$BaTiO_3$–$Bi_{0.5}Li_{0.5}TiO_3$	100–160	≈10^{-7} Scm^{-1}	3.5
$Ba_{1-x}LnTiO_3$	54–100	≈10^{-7} Scm^{-1}	2–4
$Bi_{1/2}Ti_{1/2}O_3$ doped $BaTiO_3$	125–200	≈10^{-7} Scm^{-1}	7–8

The most successful strategy for safety is to deploy PTC materials at the SEI as a protective layer, rather than generally mixing them with the cathode materials. A composite of poly(3-decylthiophene) spray coated onto an LCO cathode showed a strong PTC effect, with electronic conductivity decreasing from around 10−3 Scm−1 at room temperature to 10−6 Scm−1 at 80–100 °C, the ideal range for preventing TR.[117] However, adding the PTC materials as a separate layer comes with the disadvantages of adding bulk to the cathode, and also decreasing the conductivity at the SEI, as carbon–polymer composites are not especially conductive. A publication from 2019 used the conductive polymer poly(3-octylpyrrole)/carbon as a PTC material directly mixed into the LCO cathode material and showed increased resistivity by four orders of magnitude from room temperature to 120 °C. The 30.3 Scm−1 conductivity of the cathode at room temperature compares favorably with the 4 Scm−1 conductivity of Super P carbon.[118] Another strategy to increase conductivity is to use nickel nanoparticles in the polymer composite, which are much more conductive than carbon, leading to a 300 Scm−1 conductivity of the composite film at room temperature.[119] A practical feature of these PVdF/Ni films is that the temperature range of the PTC response can be tuned by altering the polymer/Ni ratio.

CONCLUSION

To identify the triggering reaction of thermal runway for cells undergoing fast charging, the voltage drop of full cells, the temperature rise of partial cells, and the exothermic reactions of anode material are analyzed in sequence, and the results of cells charged at high currents are as follows: (a) The voltage drop occurs after T2 of the cells is reached, unlike the fresh cells charged at low currents. This difference implies that ISCs are not involved in the thermal runaway triggering of cells after undergoing fast charging. (b) The T2 of the AnEle partial cells is close to the T2 of full cells, while the AnCa partial cells and CaEle partial cells show higher T2 values. This result suggests that the triggering reaction of thermal runaway for full cells exists in the anode−electrolyte thermodynamic system. (c) A vigorous exothermic reaction peak occurs at a lower temper-ature and consumes electrolyte when plated lithium occurs on the anode surface due to fast charging. After the plated lithium on the anode is scratched off, this reaction disappears. Besides,the reaction generates sufficient heat to trigger the thermal runaway of cells. As a result, thermal runaway of cells after fast charging is triggered by the reaction between plated lithium and electrolyte.This study reveals that fast charging, which results in severe lithium plating, should not be permitted to ensure the safety of LIBs. In the operation of LIBs, the plated lithium should be considered as its vigorous reaction with the electrolyte when the battery is overheated. Preventing thermal runaway (TR) in lithium-ion batteries can be achieved through various methods, including the use of Battery Management Systems (BMS), heat-dissipating devices, and internal cell modifications that inhibit the chemical reactions leading to TR Recent innovations, such as Phase Change Temperature (PTC) materials, capable of entering a low-conductivity state above 60 degrees Celsius, are crucial for enhancing safety by addressing the root causes of TR Future research should prioritize material engineering at the cell level to create cells resistant to TR, reducing the need for extensive safety measures in higher layers, like insulating materials and BMS.

REFERENCES

[1]. Feng, X.; Ouyang, M.; Liu, X.; Lu, L.; Xia, Y.; He, X. Thermal runaway mechanism of lithium ion battery for electric vehicles: A review. Energy Storage Mater. 2018, 10, 246–267. [Google Scholar] [CrossRef]
[2]. Yamanaka, T.; Takagishi, Y.; Tozuka, Y.; Yamaue, T. Modeling lithium ion battery nail penetration tests and quantitative evaluation of the degree of combustion risk. J. Power Sources 2019, 416, 132–140. [Google Scholar] [CrossRef]
[3]. Spotnitz, R.; Franklin, J. Abuse behavior of high-power, lithium-ion cells. J. Power Sources 2003, 113, 81–100. [Google Scholar] [CrossRef]
[4]. Ouyang, D.; Chen, M.; Liu, J.; Wei, R.; Weng, J.; Wang, J. Investigation of a commercial lithium-ion battery under overcharge/over-discharge failure conditions. RSC Adv. 2018, 8, 33414–33424. [Google Scholar] [CrossRef]
[5]. Henriksen, M.; Vågsæther, K.; Lundberg, J.; Forseth, S.; Bjerketvedt, D. Explosion characteristics for Li-ion battery electrolytes at elevated temperatures. J. Hazard. Mater. 2019, 371, 1–7. [Google Scholar] [CrossRef]
[6]. Sun, J.; Li, J.; Zhou, T.; Yang, K.; Wei, S.; Tang, N.; Dang, N.; Li, H.; Qiu, X.; Chen, L. Toxicity, a serious concern of thermal runaway from commercial Li-ion battery. Nano Energy 2016, 27, 313–319. [Google Scholar] [CrossRef]
[7]. ISO 12405-3; Electrically Propelled Road Vehicles–Test Specification for Lithium-Ion Traction Battery Packs and Systems–Part 3, Safety Performance Requirements. ISO: Geneva, Switzerland, 2014.
[8]. IEC 62133.2-2017; Secondary Cells and Batteries Containing Alkaline or Other Non—Acid Electrolytes–Safety Requirements for Portable Sealed Secondary Cells, and for Batteries Made from Them, for Use in Portable Applications—Part 2, Lithium Systems. IEC: Geneva, Switzerland, 2017.
[9]. Liu, K.; Li, K.; Peng, Q.; Zhang, C. A brief review on key technologies in the battery management system of electric vehicles. Front. Mech. Eng. 2019, 14, 47–64. [Google Scholar] [CrossRef] [Green Version]

[10]. Xia, B.; Mi, C. A fault-tolerant voltage measurement method for series connected battery packs. J. Power Sources 2016, 308, 83–96. [Google Scholar] [CrossRef]
[11]. Nascimento, M.; Ferreira, M.S.; Pinto, J.L. Real time thermal monitoring of lithium batteries with fiber sensors and thermocouples: A comparative study. Measurement 2017, 111, 260–263. [Google Scholar] [CrossRef]
[12]. Nascimento, M.; Ferreira, M.S.; Pinto, J.L. Temperature fiber sensing of Li-ion batteries under different environmental and operating conditions. Appl. Therm. Eng. 2019, 149, 1236–1243. [Google Scholar] [CrossRef]
[13]. Feng, X.; Fang, M.; He, X.; Ouyang, M.; Lu, L.; Wang, H.; Zhang, M. Thermal runaway features of large format prismatic lithium ion battery using extended volume accelerating rate calorimetry. J. Power Sources 2014, 255, 294–301. [Google Scholar] [CrossRef]
[14]. Drake, S.J.; Wetz, D.A.; Ostanek, J.K.; Miller, S.P.; Heinzel, J.M.; Jain, A. Measurement of anisotropic thermophysical properties of cylindrical Li-ion cells. J. Power Sources 2014, 252, 298–304. [Google Scholar] [CrossRef]
[15]. Zhu F, Du X, Lei J, Audisio L, Sypeck D. Experimental study on the crushing behaviour of lithium-ion battery modules. Int J Crashworthiness 2020:1–10. https://doi.org/10.1080/13588265.2020.1766397
[16]. Hu LL, Zhang ZW, Zhou MZ, Zhang HJ. Crushing behaviors and failure of packed batteries. Int J Impact Eng 2020;143. https://doi.org/10.1016/j.ijimpeng.2020.103618
[17]. Yamauchi T, Mizushima K, Satoh Y, Yamada S. Development of a simulator for both propertyand safety of a lithium secondary battery. J Power Sources 2004; 136:99–107. https://doi.org/10.1016/J.JPOWSOUR.2004.05.011
[18]. Maleki H, Howard JN. Internal short circuit in Li-ion cells. J Power Sources 2009; 191:568–74. https://doi.org/10.1016/J.JPOWSOUR.2009.02.070
[19]. Zavalis TG, Behm M, Lindbergh G. Investigation of Short-Circuit Scenarios in a Lithium-Ion Battery Cell. J Electrochem Soc 2012;159:A848 https://doi.org/10.1149/2.096206JES
[20]. Zhao R, Liu J, Gu J. Simulation and experimental study on lithium ion battery short circuit. Appl Energy 2016;173:29–39.https://doi.org/10.1016/j.apenergy.2016.04.016
[21]. Zhu F, Zhou R, Sypeck D, Deng J, Bae C. Failure behavior of prismatic Li-ion battery cells under abuse loading condition - A combined experimental and computational study. J Energy Storage 2022;48:103969 https://doi.org/10.1016/J.EST.2022.103969
[22]. Leising RA, Palazzo MJ, Takeuchi ES, Takeuchi KJ. Abuse Testing of Lithium-Ion Batteries: Characterization of the Overcharge Reaction of LiCoO2/Graphite Cells. J Electrochem Soc 2001;148:A838https://doi.org/10.1149/1.1379740
[23]. Spotnitz R, Franklin J. Abuse behavior of high-power, lithium-ion cells. J Power Sources 2003;113:81–100. https://doi.org/10.1016/S0378-7753(02)00488-3
[24]. Zeng Y, Wu K, Wang D, Wang Z, Chen L. Overcharge investigation of lithium-ion polymer batteries. J Power Sources 2006;160:1302–7. https://doi.org/10.1016/j.jpowsour.2006.02.009
[25]. Ye J, Chen H, Wang Q, Huang P, Sun J, Lo S. Thermal behavior and failure mechanism of lithium ion cells during overcharge under adiabatic conditions. Appl Energy 2016;182:464–74. https://doi.org/10.1016/j.apenergy.2016.08.124
[26]. Ohsaki T, Kishi T, Kuboki T, Takami N, Shimura N, Sato Y, et al. Overcharge reaction of lithium-ion batteries. J Power Sources 2005;146:97–100. https://doi.org/10.1016/j.jpowsour.2005.03.105
[27]. Yuan QF, Zhao F, Wang W, Zhao Y, Liang Z, Yan D. Overcharge failure investigation of lithium-ion batteries. Electrochim Acta 2015;178:682–8. https://doi.org/10.1016/j.electacta.2015.07.147
[28]. Mao N, Wang ZR, Chung YH, Shu CM. Overcharge cycling effect on the thermal behavior, structure, and material of lithium-ion batteries. Appl Therm Eng 2019; 163:114147.https://doi.org/10.1016/j.applthermaleng.2019.114147
[29]. Hamisi CM, Chombo PV, Laoonual Y, Wongwises S. An Electrothermal Model to Predict Thermal Characteristics of Lithium-Ion Battery under Overcharge Condition. Energies (Basel) 2022;15. 10.3390/EN15062284.
[30]. Yeh WT, Huang YF, Wu CC, da Hong P. Structure and morphological changes of multilayer separators for lithium-ion batteries under abuse/overcharge conditions. J Appl Polym Sci 022;139:52046.https://doi.org/10.1002/APP.52046
[31]. Feng X, Fang M, He X, Ouyang M, Lu L, Wang H, et al. Thermal runaway features of large format prismatic lithium ion battery using extended volume accelerating rate calorimetry. J Power Sources 2014;255:294–301. https://doi.org/10.1016/j.jpowsour.2014.01.005
[32]. Wu T, Chen H, Wang Q, Sun J. Comparison analysis on the thermal runaway of lithium-ion battery under two heating modes. J Hazard Mater 2018;344:733–41.https://doi.org/10.1016/j.jhazmat.2017.11.022
[33]. Zhao C, Sun J, Wang Q. Thermal runaway hazards investigation on 18650 lithium-ion battery using extended volume accelerating rate calorimeter.J Energy Storage 2020;28:101232.https://doi.org/10.1016/j.est.2020.101232
[34]. Kelkar, Y. Dasari, S. S. Williamson, in 2020 IEEE Int. Conf. Power Electronics Smart Grid Renewable Energy, PESGRE 2020, Institute Of Electrical And Electronics Engineers Inc., Piscataway, NJ 2020. Google Scholar
[35]. Anthony, D. Wong, D. Wetz, A. Jain, Int. J. Heat Mass Transf. 2017, 111, 223. Web of Science®Google Scholar
[36]. Xiao, IEEE Trans. Ind. Electron. 2015, 62, 3112. Web of Science®Google Scholar
[37]. Abada, M. Petit, A. Lecocq, G. Marlair, V. Sauvant-Moynot, F. Huet, J. Power Sources 2018, 399, 264.CASWeb of Science®Google Scholar
[38]. Feng, S. Zheng, D. Ren, X. He, L. Wang, H. Cui, X. Liu, C. Jin, F. Zhang, C. Xu, H. Hsu, S. Gao, T. Chen, Y. Li, T. Wang, H. Wang, M. Li, M. Ouyang, Appl. Energy 2019, 246, 53.CASWeb of Science®Google Scholar
[39]. Huang, C. Yao, B. Mao, Q. Wang, J. Sun, Z. Bai, Energy 2020, 213, 119082. CASWeb of Science®Google Scholar
[40]. Esho, K. Shah, A. Jain, Appl. Therm. Eng. 2018, 145, 287.CASWeb of Science®Google Scholar

[41]. Leng, C. M. Tan, M. Pecht, Sci. Rep. 2015, 5, 12967. CASPubMedWeb of Science®Google Scholar
[42]. Ren, X. Liu, X. Feng, L. Lu, M. Ouyang, J. Li, X. He, Appl. Energy 2018, 228, 633. CASWeb of Science®Google Scholar
[43]. Wang, E. Lara-Curzio, E. T. Rule, C. S. Winchester, J. Power Sources 2017, 342, 913.Google Scholar
[44]. Leng, C. M. Tan, M. Pecht, Sci. Rep. 2015, 5, 12967. CASPubMedWeb of Science®Google Scholar
[45]. A. Howey, V. Yufit, P. D. Mitcheson, G. J. Offer, N. P. Brandon, in 2013 World Electric Vehicle Symp. and Exhibition, EVS 2014, Institute of Electrical and Electronics Engineers Inc., Piscataway, NJ 2014. Google Scholar
[46]. Riviere, A. Sari, P. Venet, F. Meniere, Y. Bultel, Batteries 2019, 5, 37. CASGoogle Scholar
[47]. Weng, Y. Cui, J. Sun, H. Peng, J. Power Sources 2013, 235, 36. CASWeb of Science®Google Scholar
[48]. Zheng, J. Zhu, D. D. C. Lu, G. Wang, T. He, Energy 2018, 150, 759. Web of Science®Google Scholar
[49]. Ma, Y. Wang, Q. Duan, T. Wu, J. Sun, Q. Wang, Energy 2018, 164, 745. Web of Science®Google Scholar
[50]. Petzl, M. A. Danzer, J. Power Sources 2014, 254, 80. CASWeb of Science®Google Scholar
[51]. Rowden, N. Garcia-Araez, in Energy Reports, Elsevier Ltd, Amsterdam 2020, pp. 10–18. Google Scholar
[52]. E.Galushkin, N. N. Yazvinskaya, D. N. Galushkin, J. Electrochem. Soc. 2019, 166, A897. CASWeb of Science®Google Scholar
[53]. Pan, X. Feng, L. Lu, M. Ouyang, ECS Meet. Abstr. 2019, MA2019-01, 590. Google Scholar
[54]. Wenger, R. Waller, V. R. H. Lorentz, M. Marz, M. Herold, in IECON Proc., Industrial Electronics Conf., Institute of Electrical and Electronics Engineers Inc., Piscataway, NJ 2014, pp. 5654–5659. Google Scholar
[55]. Sturk, L. Rosell, P. Blomqvist, A. AhlbergTidblad, Batteries 2019, 5, 61.12J. Kudrnovsky, G. Bouzerar, I. Turek, Appl. Phys. Lett. 2007, 91, 102509. Google Scholar
[56]. Yu, Q. Li, Ceram. Int. 2020, 46, 8796. CASWeb of Science®Google Scholar
[57]. Amirah, T. Sulong, R. Aina, M. Osman, M. S. Idris, Z. Azhar, Z. Jamal, EPJ Web Conf. 2017, 162, 01050. Web of Science®Google Scholar
[58]. Zhang, H. Li, S. Wang, Y. Cao, H. Yang, X. Ai, F. Zhong, J. Energy Chem. 2020, 44, 33.Web of Science®Google Scholar
[59]. Shi, X. Cai, W. Wang, G. Wang, Macromol. Chem. Phys. 2020, 221, 2000144.CASWeb of Science®Google Scholar
[60]. Yang, Z. Peng, C. Wang, X. Fu, Ceram. Int. 2016, 42, 17792.CASWeb of Science®Google Scholar
[61]. Huo, Y. Qu, Sensors Actuators, A 2006, 128, 265.